Available online at www.sciencedirect.com
SCIENCE DIRECT®
Bioorganic & Medicinal Chemistry Letters 15 (2005) 5129–5135
Bioorganic & Medicinal Chemistry Letters

Structural basis for the GSK-3β binding affinity and selectivity against CDK-2 of 1-(4-aminofurazan-3yl)-5-dialkylaminomethyl-1-*H*-[1,2,3] triazole-4-carboxylic acid derivatives

Vineet Pande and Maria J. Ramos*

REQUIMTE, Departamento de Química, Faculdade de Ciências, Universidade do Porto, Rua do Campo Alegre 687, 4169-007 Porto, Portugal

Received 13 July 2005; revised 22 August 2005; accepted 23 August 2005

Abstract—A novel structural class of glycogen synthase kinase-3β inhibitors is modeled using quantum mechanics, automated docking, and molecular dynamics simulations. The proposed binding modes identify important hydrogen bonds and salt-bridges with the ATP-binding pocket of the kinase. The modeled complexes justify the observed structure–activity relationships and provide a structural basis for the high selectivity of these inhibitors against cyclin dependent kinase-2.

Alzheimer's disease, diabetes type-2, and tumorigenesis are important examples of disorders, where glycogen synthase kinase-3 (GSK-3), is involved. A serine/threonine kinase, GSK-3, is ubiquitously expressed in mammalian tissues and interferes with a plethora of cellular and physiological processes including glycogen metabolism, τ-phosphorylation, Wnt signaling, and NF-κB pathway.[1–3] Because many disorders are associated with protein phosphorylation abnormalities, discovery of pharmacological inhibitors of kinases and phosphatases in general,[4] and GSK-3 in particular,[5] has emerged as a tempting goal in drug research.

GSK-3 has two major isoforms (α and β), which are 98% identical within the catalytic domain,[6] however, GSK-3β has received more attention in pharmacological and structural studies. Consequently, more than 30 inhibitors of GSK-3β have been described,[5] most of them being ATP-competitive and some with IC_{50} values in the nanomolar range. Examples include staurosporine, paullones, indirubins, hymenialdisine, SB-415286, CHIR98023, etc. Important in kinase inhibition is the ability of an inhibitor to be specific for a given kinase or set of kinases. This is even more challenging due to the structural similarity of the ATP-binding site of all kinases. In the case of GSK-3β, it is often desirable to achieve selectivity against the cyclin dependent kinases (CDKs), since GSK-3β is phylogenetically most closely related to the CDKs.[1] All the different classes of compounds reported[5] have shown a limited degree of GSK-3β specificity. However, recently a new structural class of ATP-competitive 1-(4-aminofurazan-3yl)-5-dialkylaminomethyl-1*H*-[1,2,3] triazole-4-carboxylic acid derivatives were reported,[7] which not only have high affinity for GSK-3β besides desirable water solubility, but apparently have the highest level of selectivity against CDK-2 amongst all the GSK-3β inhibitors published until now.

The structure–activity relationships (SARs)[7] in this novel class of GSK-3β inhibitors are focused around two major substructural classes (Fig. 1; nomenclature for inhibitors is the same as used in the experimental study by Olesen et al.[7] for the sake of compatibility). However, no structural information is available on the possible binding mode of these inhibitors which apparently do not fit into any other previously co-crystallized or modeled kinase inhibitors. The present study reports a possible binding mode of this novel class of inhibitors in the GSK-3β active-site, using quantum mechanics, automated docking, and molecular dynamics simulations.

The three-dimensional structure of GSK-3β was obtained from the protein data bank (pdb code: 1j1b), which is a crystallographic structure of the kinase bound to ANP at 1.80 Å resolution, with a *R* value of 0.216.[8]

Keywords: Glycogen synthase kinase-3β; Cyclin dependent kinase-2; Docking; Molecular dynamics; Selectivity.
* Corresponding author. Tel.: +351 226082806; fax: +351 226082959; e-mail: mjramos@fc.up.pt

0960-894X/$ - see front matter © 2005 Elsevier Ltd. All rights reserved.
doi:10.1016/j.bmcl.2005.08.077

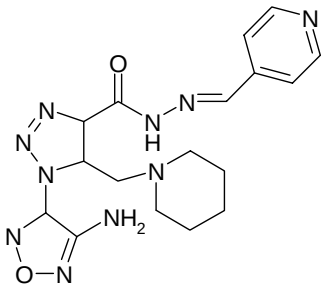

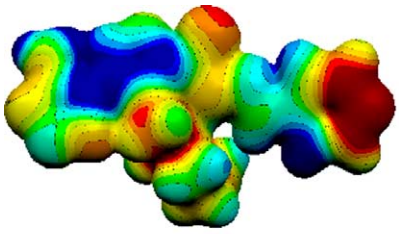

Compound 6b
IC_{50}(GSK-3β) = 0.10
IC_{50}(CDK-2) = 96

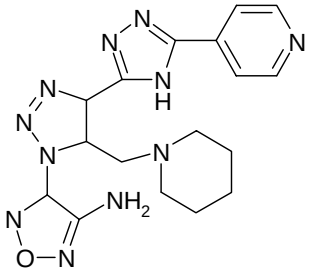

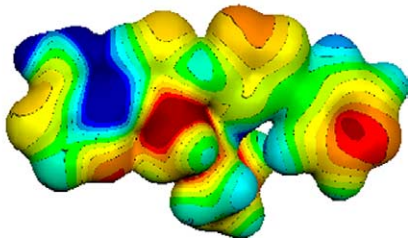

Compound 8b
IC_{50}(GSK-3β) = 0.28
IC_{50}(CDK-2) = >250

Figure 1. 1-(4-Aminofurazan-3yl)-5-dialkylaminomethyl-1*H*-[1,2,3] triazole-4-carboxylic acid derivatives, compound **6b** and compound **8b**.[7] IC_{50} values in micromolars are shown for both GSK-3β and CDK-2. MEPs representing a maximum potential, $\phi_+ = 0.10$ a.u., and a minimum potential, $\phi_- = -0.10$ a.u., are mapped onto electron density isosurfaces of $\rho = 0.009$ e/Å.[3] Negative potentials are in red color and positive in blue. MOLEKEL 4.3 package was used to obtain the maps after calculating the electron density.

It has been justified in recent studies that ATP or ANP bound kinase structures are better starting points to model ATP competitive molecules than apo structures.[9,10] Quantum mechanical calculations were performed on the compounds first to optimize their geometries and then to obtain molecular electrostatic potentials (MEPs). These calculations were performed using the density functional theory (B3LYP functional and 6-31 + G(d) basis set) as implemented in the Gaussian 03 program.[11] Figure 1 depicts the MEPs for compounds **6b** and **8b**. Relative electropositive potential is saturated toward the aminofurazan part, whereas the electronegative potential is denser toward the 4-pyridyl moiety. Automated docking studies were performed using GOLD 2.0 program,[12] with the ATP-binding pocket of GSK-3β defined as active site (see Supporting Information for details of protocol). The most populated docking solutions for compounds **6b** and **8b** also conformed to their MEPs, allowing us to choose a docking mode with electronegative part (4-pyridyl end) occupying the triphosphate subsite in the ATP-binding pocket and electropositive part (aminofurazan end) occupying the adenine subsite (Fig. 2).

Since **6b** is the most potent analog and **8b** the most selective one,[7] detailed studies were further performed on docked complexes of these two compounds, which are expected to capture the most essential and representative interactions in the whole series. Molecular dynamics simulations were carried out for each complex to assess their stability and behavior and to account for ligand induced conformational changes in the kinase. Duan (ff03)[13] and general amber force fields[14] were used for the protein and the ligands, respectively. Simulations were performed using the SANDER module of AMBER 8.0 package.[15] Point charges for the ligands were calculated using the AM1-BCC (AM1 Hamiltonian with bond charge correction) method.[16] Unrestrained molecular dynamics simulations were performed in aqueous solution for each complex at constant temperature and pressure with the application of periodic boundary conditions. Protocol involved 500 ps of equilibration phase followed by a 700 ps production phase. Final 400 ps of trajectories were used to calculate the average coordinates of each complex. These average structures were then energy minimized (see Supporting Information for details of simulation and minimization protocols). These final models are depicted in Figure 2. Analysis of trajectories was done with the PTRAJ module of AMBER 8.0.[15] Figure 3 shows the evolution of root-mean-square deviation (rmsd) of the coordinates. The time averages of important hydrogen bonds and

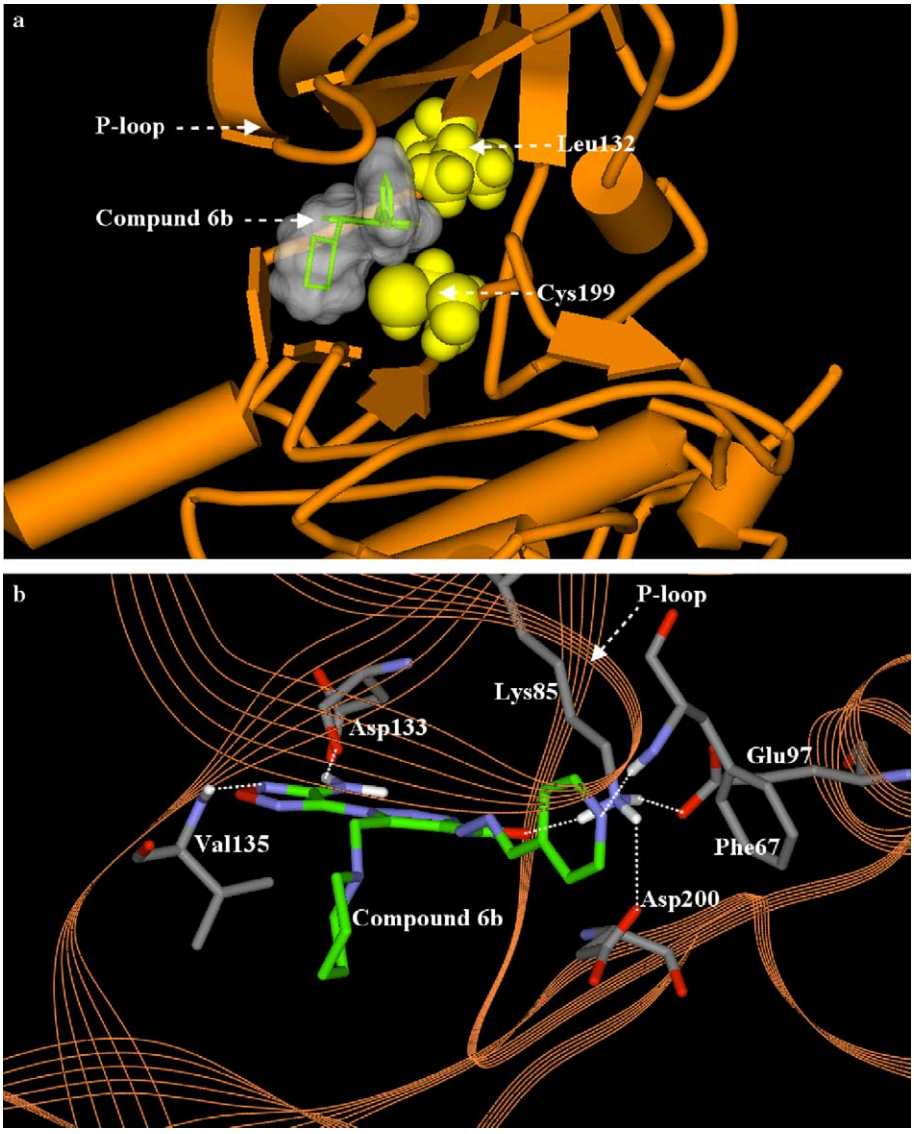

Figure 2. Proposed binding mode for inhibitors **6b** (a and b) and **8b** (c and d) in the GSK-3β active site from the average calculated structure. (a and c) Inhibitors are shown with their soft-surfaces (drawn using DS Viewer Pro 6.0 package, Accelrys, San Diego, CA) depicting the fit in the ATP binding pocket, under the P-loop, while contacting, Leu132 and Cys199 residues (shown in yellow, as CPK drawing). (b and d) Calculated hydrogen bonds and salt-bridges are depicted (broken lines). For clarity only hydrogens bonded to donors and residues involved in these interactions are shown. Inhibitor carbon atoms are in green, while protein carbons are shown in gray color. All nitrogen atoms are in blue, hydrogens in white, and oxygen atoms in red color.

salt-bridges (electrostatic interactions) are shown in Table 1 (see Supporting Information for time evolution of these distances and angles).

Both **6b** and **8b** have an internal hydrogen bond between their piperidine nitrogens and the amide nitrogen in **6b** and triazole nitrogen in **8b**, respectively. During the entire simulation, the ligands hence did not show any major conformational change as can be seen from their individual rmsds (Fig. 3). The tightly bound inhibitors are stabilized with the aid of hydrogen bonds and salt-bridges, besides van der Waals interactions with the GSK-3β active site residues. The ATP-binding pocket is occupied fully due to the elongated structure of these inhibitors. Especially the Leu132 and Cys199 residues provide dimpled and bulged contours to the active site, respectively (Figs. 2 and 5). Important are the hydrogen bonds made with the backbone atoms of Asp133 and Val135 residues by both **6b** and **8b** (Fig. 2). In fact, these two residues have been known to contribute to equivalent hydrogen bonds in all the GSK-3β inhibitor complexes proposed[5] including paullones, indirubin-3′-oxime, staurosporine, ARA 014418, and pyrazolopyridine **9**, etc. In the case of **6b**, a third hydrogen bond is observed between the backbone amide nitrogen of Phe67 and the 4-pyridyl nitrogen of the inhibitor. Significant is the observation that this hydrogen bond is a part of the conformational change brought in the P-loop (glycine-rich loop) of the kinase by the inhibitor, as in the starting complex it was absent (see time evolution of this interaction in Supporting Information). The 4-pyridyl ring in **6b** also contributes to van der Waals

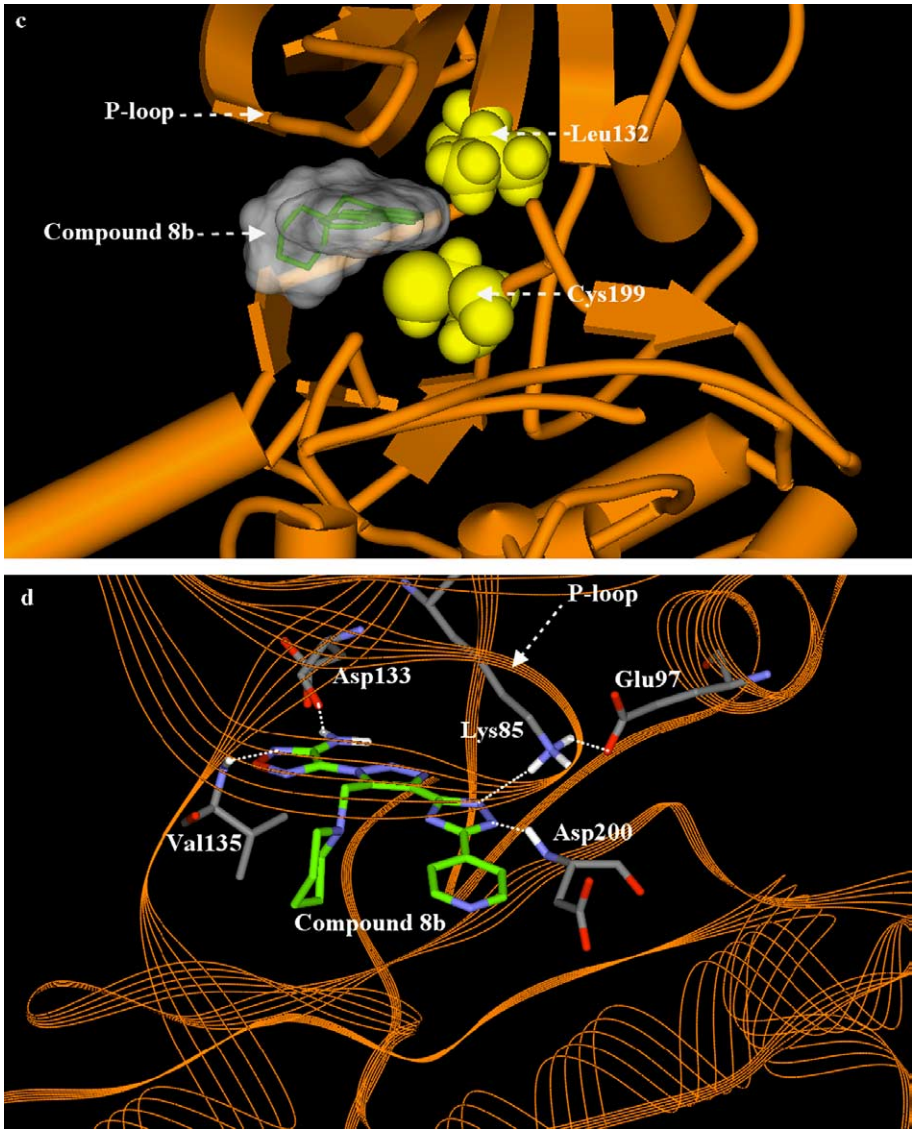

Figure 2. *(continued)*

interactions with the phenyl ring of Phe67 (Fig. 2b). However, in the case of **8b**, due to its conformation, the 4-pyridyl nitrogen remains exposed to the solvent. Nevertheless, a hydrogen bond, though not so strong, is observed between one of the nitrogens of the triazole ring and backbone amide nitrogen of Asp200. These differences account possibly for the weaker inhibition potency of **8b** when compared to **6b**.

One of the interesting results of our simulation study is the identification of stable, multiple electrostatic interactions via Lys85 residue of GSK-3β. In both **6b** and **8b**, this lysine is observed to form very stable salt-bridges, simultaneously, with the inhibitor and Glu97, thus providing a unique electrostatic bridge in one end of binding pocket (time evolution plots in Supplementary Material). This is expected to be very significant in molecular recognition of these inhibitors by the kinase. Further, in the case of **6b**, due to allowed space in the binding site, Lys85 is also observed to make a third simultaneous salt bridge with Asp200. This electrostatic interaction, however, is expected to be not as significant and potent as the one with Glu97, because Asp200 is a solvent exposed residue whereas Glu97 is relatively more buried. A comparative solvation shell analysis during the entire simulation justifies this fact (Fig. 4) as it is observed that in the case of both compounds **6b** and **8b**, Asp200 residue is more solvent exposed as compared to Glu97 during the entire length of simulation. Further, the Asp200 residue, not being buried in the protein matrix, was found to be very flexible (see Supplementary Material).

The proposed binding mode clearly justifies the observed SAR,[7] thus validating the models. Since less potent inhibitors showed mixed docking modes, without any clear signal, it is important to understand why they do not bind in the same way as the good ones, by using the binding characteristics observed in the latter. To understand why less potent inhibitors hit or miss in the GSK-3β active site, we superimposed them using docking model of **6b** as a template (examples for **4b**

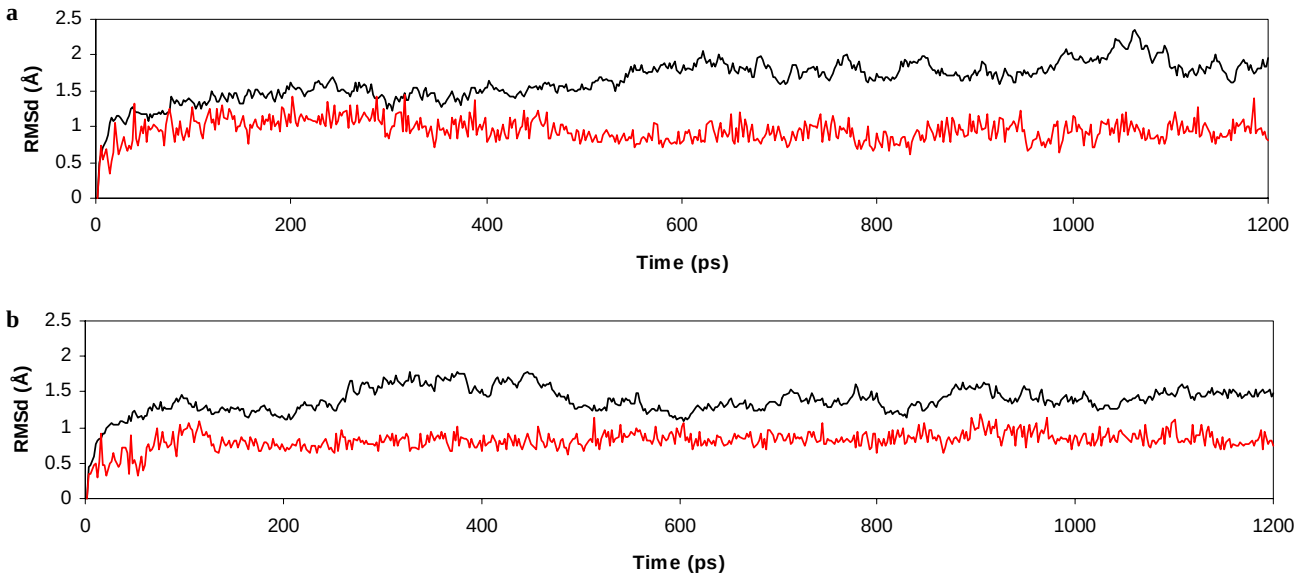

Figure 3. Evolution of the rmsd of the C_α atoms (black) of (a) GSK-3β:**6b** complex, and (b) GSK-3β:**8b** complex, with respect to the initial structure. Shown in red is the rmsd of the ligand alone. Each line is made up of 600 individual points from the trajectory.

Table 1. Hydrogen bonds and salt-bridges involved in complexes during the molecular dynamics simulation[a]

Interaction	Mean distance[b] (Å) ± standard deviation	Mean angle[c](degree) ± standard deviation
GSK-3β:**6b**		
Phe67(N):6b	3.21 ± 0.21	156.62 ± 10.12
Asp133(O):6b	2.90 ± 0.15	152.86 ± 10.24
Val135(N):6b	3.07 ± 0.16	146.50 ± 14.15
Lys85(NZ):6b	2.91 ± 0.15	
Lys85(NZ):Glu97(OE1)	2.78 ± 0.12	
Lys85(NZ):Asp200(OD2)	3.15 ± 0.77	
GSK-3β:**8b**		
Asp133(O):8b	2.90 ± 0.13	157.43 ± 9.44
Val135(N):8b	3.05 ± 0.15	148.43 ± 13.69
Asp200(N):8b	3.95 ± 0.42	133.67 ± 13.7
Lys85(NZ):8b	3.05 ± 0.15	
Lys85(NZ):Glu97(OE1)	2.86 ± 0.19	

[a] Calculated average of the production phase (350 data points).
[b] Measured between heavy atoms.
[c] Measured between donor, hydrogen, and acceptor.

and **7b**, which show at least half an order of magnitude weaker activity compared to **6b** and **8b**, are shown in Supplementary Material). For instance, in case of **4b** the electrostatic nature of the inhibitor will change without the presence of electronegative pyridyl moiety, which is likely to interfere with the Lys85 interaction (NH_2 interacting with NH_3). Further, smaller size of **4b** would also render the P-loop more flexible and would perhaps let it close more than normal. Next, for **7b**, its extended length, as well as a preferred staggered conformation along the CH_2–CH_2 group attached between the amide and 4-pyridyl groups, render it a conformation which has bumps with the active site roof, that is, the P-loop (Gly65 residue, especially). Besides this, it also has bumps with the Lys85 and Phe67 side chains. In case Lys85 or Phe67 swap away, **7b** will lose interactions, besides, if the inhibitor itself rotates around to adjust, it will have an unfavorable internal energy due to the loss of staggered conformation mentioned above, besides an energy barrier accounting for the rotation.

The models also explain, why possibly these compounds are selective for GSK-3β, in comparison to CDK-2. Figure 5 shows the active sites of the two kinases (following a three-dimensional superposition of the two kinases in Insight II modeling program) comparing 'selectivity residues' (CDK-2 structure is PDB ID: 1hck[17] (bound to ATP) and GSK-3β structure is PDB ID: 1j1b[8] (bound to ANP)). The buried residue in CDK-2 equivalent to Glu97 of GSK-3β is Leu148 (in three-dimensional superposition and not sequence alignment), although an equivalent of GSK-3β's Lys85 (Lys33 in CDK-2) is present. This implies that the unique salt bridge network in CDK-2 will be missed by **6b** and **8b**. Further, the differences in the active site topologies owing to Phe80 and Ala144 residues in CDK-2 may also impart selectivity to

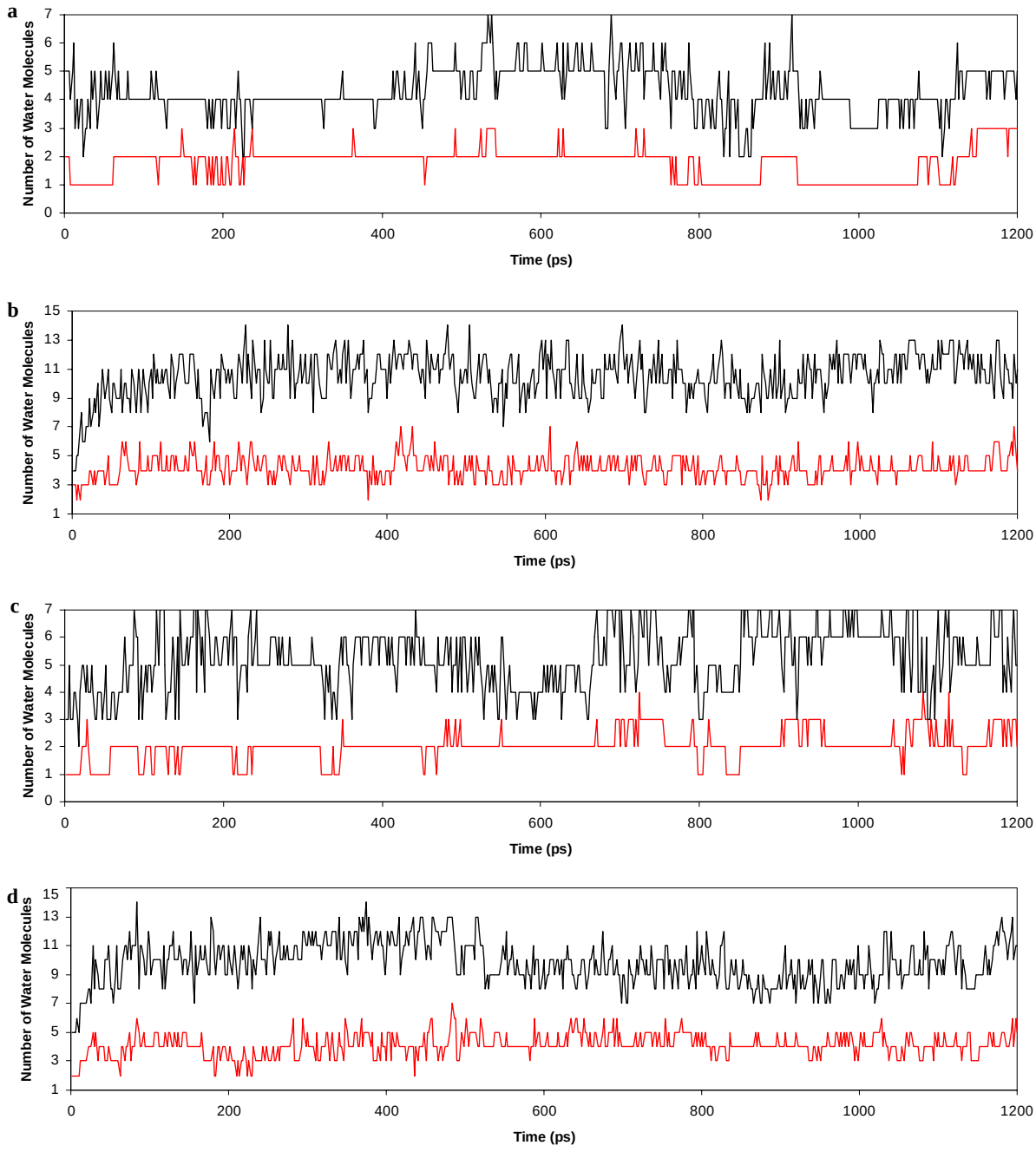

Figure 4. Solvation shells describing the number of solvent water molecules occupied around the side chains of (a) Glu97 and (b) Asp200 in GSK-3β:**6b** complex, and (c) Glu97 and (d) Asp200 in GSK-3β:**8b** complex. First solvation shell (total water molecules <3.4 Å) is shown in red color and second solvation shell (total water molecules <5.0 Å) in black.

the inhibitors. Since **6b** and **8b** are elongated inhibitors, binding tightly to the ATP-binding pocket and occupying the adenine, ribose, as well as triphosphate subsites, in CDK-2, they may not be able to easily adjust themselves, without losing hydrogen bonds in the tail and the head when they miss the specific interactions or have unfavorable interactions postulated above.

Acknowledgments

This work was supported by the National Foundation for Cancer Research, USA (Ph.D. scholarship for VP by NFCR Center for Computational Drug Discovery, University of Oxford, UK), and Fundação para a Ciência e a Tecnologia, Portugal.

Supplementary material

Detailed protocols for docking and molecular dynamics simulations, plots of time evolution of hydrogen bonds, salt-bridges, solvation shells and molecular models for compound **4b** and **7b** binding are provided as supplementary data and can be found, in the online version at doi:10.1016/j.bmcl.2005.08.077.

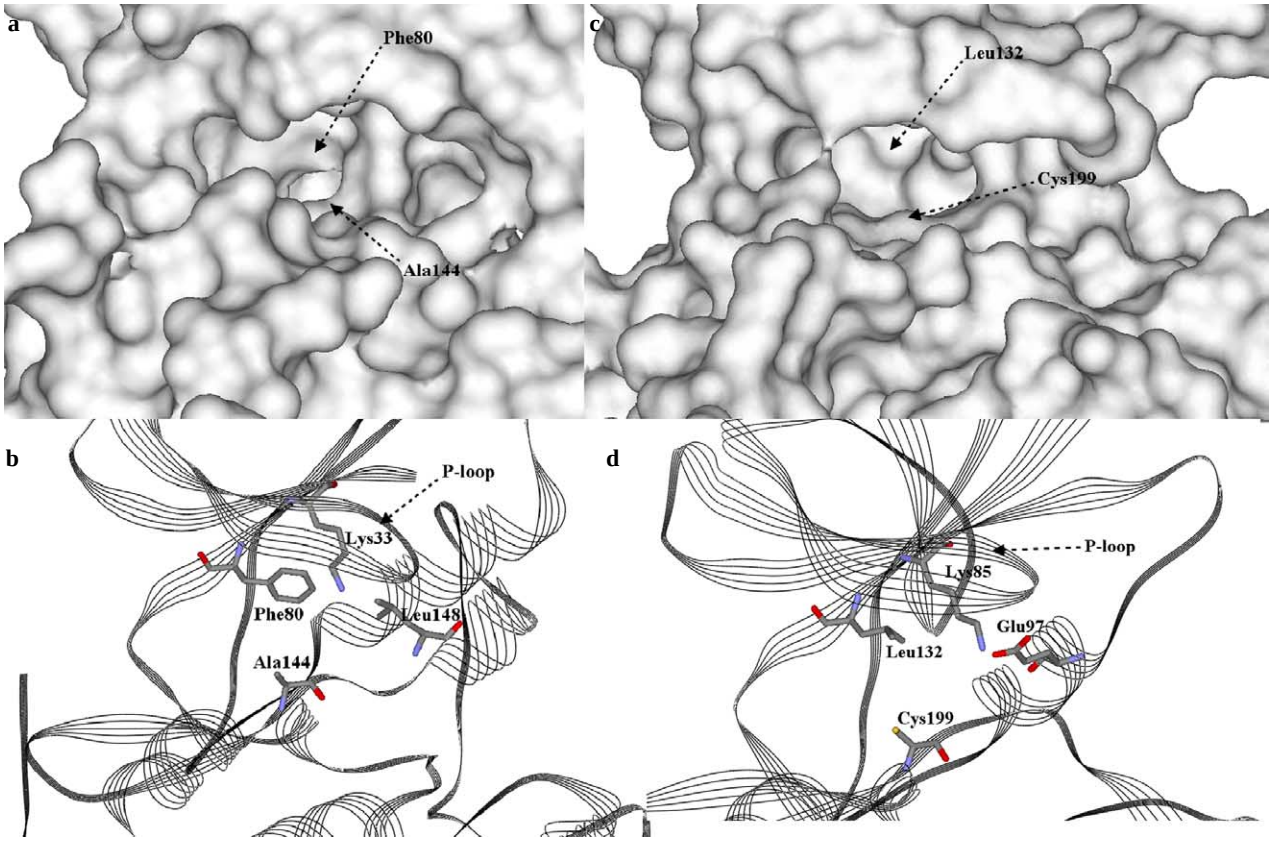

Figure 5. Active-site pockets of (a and b) CDK-2 and (c and d) GSK-3β. Solvent-exposed surfaces (drawn using a probe of 1.4 Å radius, using DS Viewer Pro 6.0 package, Accelrys Inc., San Diego, CA) are shown (a and c), highlighting the differential topologies of the two active sites. (b and d) depict the active sites, while showing (only heavy atoms; carbon atoms in gray, oxygen atoms in red, sulfur atom in yellow, and nitrogen atoms in blue) of 'selectivity residues.'

References and notes

1. Frame, S.; Cohen, P. *Biochem. J.* **2001**, *359*, 1.
2. Doble, B. W.; Woodgett, J. R. *J. Cell Sci.* **2003**, *116*, 1175.
3. Jope, R. S.; Johnson, G. V. W. *Trends Biochem. Sci.* **2004**, *29*, 95.
4. Cohen, P. *Nat. Rev. Drug Discov.* **2002**, *1*, 309.
5. Meijer, L.; Flajolet, M.; Greengard, P. *Trends Pharmacol. Sci.* **2004**, *25*, 471.
6. Ali, A.; Hoeflich, K. P.; Woodgett, J. R. *Chem. Rev.* **2001**, *101*, 2527.
7. Olesen, P. H.; Sørensen, A. R.; Ursø, B.; Kurtzhals, P.; Bowler, A. N.; Ehrbar, U.; Hansen, B. F. *J. Med. Chem.* **2003**, *46*, 3333.
8. Aoki, M.; Yokota, T.; Sasaki, C.; Hasegawa, T.; Okumura, C.; Kohno, T.; Sugio, S.; Matsuzaki, T.; Okumura, C.; Kohno, T.; Sugio, S.; Matsuzaki, T. Submitted for publication.
9. Rockey, W. H.; Elcock, A. H. *Proteins* **2002**, *48*, 664.
10. Gould, C.; Wong, C. F. *Pharmacol. Ther.* **2002**, *93*, 169.
11. Frisch, M. J.; Trucks, G. W.; Schlegel, H. B.; Scuseria, G. E.; Robb, M. A.; Cheeseman, J. R.; Montgomery, J. A., Jr.; Vreven, T.; Kudin, K. N.; Burant, J. C.; Millam, J. M.; Iyengar, S. S.; Tomasi, J.; Barone, V.; Mennucci, B.; Cossi, M.; Scalmani, G.; Rega, N.; Petersson, G. A.; Nakatsuji, H.; Hada, M.; Ehara, M.; Toyota, K.; Fukuda, R.; Hasegawa, J.; Ishida, M.; Nakajima, T.; Honda, Y.; Kitao, O.; Nakai, H.; Klene, M.; Li, X.; Knox, J. E.; Hratchian, H. P.; Cross, J. B.; Bakken, V.; Adamo, C.; Jaramillo, J.; Gomperts, R.; Stratmann, R. E.; Yazyev, O.; Austin, A. J.; Cammi, R.; Pomelli, C.; Ochterski, J. W.; Ayala, P. Y.; Morokuma, K.; Voth, G. A.; Salvador, P.; Dannenberg, J. J.; Zakrzewski, V. G.; Dapprich, S.; Daniels, A. D.; Strain, M. C.; Farkas, O.; Malick, D. K.; Rabuck, A. D.; Raghavachari, K.; Foresman, J. B.; Ortiz, J. V.; Cui, Q.; Baboul, A. G.; Clifford, S.; Cioslowski, J.; Stefanov, B. B.; Liu, G.; Liashenko, A.; Piskorz, P.; Komaromi, I.; Martin, R. L.; Fox, D. J.; Keith, T.; Al-Laham, M. A.; Peng, C. Y.; Nanayakkara, A.; Challacombe, M.; Gill, P. M. W.; Johnson, B.; Chen, W.; Wong, M. W.; Gonzalez, C.; Pople, J. A.; Gaussian 03, Revision C.02, Gaussian, Wallingford, CT, 2004.
12. GOLD 2.0, CCDC Software Ltd. Cambridge, U.K.
13. Duan, Y.; Wu, C.; Chowdhury, S.; Lee, M. C.; Xiong, G.; Zhang, W.; Yang, R.; Cieplak, P.; Luo, R.; Lee, T. *J. Comput. Chem.* **2003**, *24*, 1999.
14. Wang, J.; Wolf, R. M.; Caldwell, J. W.; Kollman, P. A.; Case, D. A. *J. Comput. Chem.* **2004**, *25*, 1157.
15. Case, D. A.; Darden, T. A.; Cheatham, T. E. III.; Simmerling, C. L.; Wang, J.; Duke, R. E.; Luo, R.; Merz, K. M.; Wang, B.; Pearlman, D. A.; Crowley, M.; Brozell, S.; Tsui, V.; Gohlke, H.; Mongan, J.; Hornak, V.; Cui, G.; Beroza, P.; Schafmeister, C.; Caldwell, J. W.; Ross, W. S.; Kollman, P. A. AMBER 8.0, University of California, San Francisco, 2004.
16. (a) Jakalian, A.; Bush, B. L.; Jack, D. B.; Bayly, C. I. *J. Comput. Chem.* **2000**, *21*, 132; (b) Jakalian, A.; Jack, D. B.; Bayly, C. I. *J. Comput. Chem.* **2002**, *23*, 1623.
17. Schulze-Gahmen, U.; Brandsen, J.; Jones, H. D.; Morgan, D. O.; Meijer, L.; Vesley, J.; Kim, S. H. *Proteins* **1995**, *22*, 378.